Journal of Materials Chemistry B

ROYAL SOCIETY OF CHEMISTRY

PAPER

View Article Online
View Journal | View Issue

Cite this: J. Mater. Chem. B, 2023, 11, 4914

Electrokinetic transport properties of deoxynucleotide monophosphates (dNMPs) through α-phase phosphorene carbide nanochannel for electrophoretic detection

Xiao Jia, [a] Xiaohang Lin, *[b] Yang Liu, [a] Yuanyuan Qu, [a] Mingwen Zhao, [a] Xiangdong Liu*[a] and Weifeng Li *[a]

Electrokinetic identification of biomolecules is an effective analytical method in which an electric field drives the nucleic acids, peptides, and other species through a nanoscale channel and the time of flight (TOF) is recorded. The mobilities of the molecules are determined by the water/nanochannel interface, including the electrostatic interactions, surface roughness, van der Waals interactions, and hydrogen bonding. The recently reported α-phase phosphorus carbide (α-PC) has an intrinsically wrinkled structure that can efficiently regulate the migrations of biomacromolecules on it, making it a highly promising candidate for the fabrication of nanofluidic devices for electrophoretic detection. Herein, we studied the theoretical electrokinetic transport process of dNMPs in α-PC nanochannel. Our results clearly show that the α-PC nanochannel can efficiently separate dNMPs in a wide range of electric field strengths from 0.5 to 0.8 V nm^{-1}. The electrokinetic speed order is deoxy thymidylate monophosphates (dTMP) > deoxy cytidylate monophosphates (dCMP) > deoxy adenylate monophosphates (dAMP) > deoxy guanylate monophosphates (dGMP) and is almost independent of the electric field strength. For a nanochannel with a typical height of 3.0 nm and an optimized electric field of 0.7–0.8 V nm^{-1}, the difference in TOF is large enough to guarantee accurate identification. We find that dGMP is the weakest link among the four dNMPs for sensitive detection in the experiment because its velocity always shows large fluctuations. This is because of its significantly different velocities when dGMP is bound to α-PC in different orientations. In contrast, for the other three nucleotides, the velocities are independent of the binding orientations. The high performance of the α-PC nanochannel is attributed to its wrinkled structure in which the nanoscale grooves can form nucleotide-specific interactions that greatly regulate the transport velocities of the dNMPs. This study illustrates the high potential of α-PC for electrophoretic nanodevices. This could also provide new insights for the detection of other types of biochemical or chemical molecules.

Received 3rd March 2023,
Accepted 3rd May 2023

DOI: 10.1039/d3tb00460k

rsc.li/materials-b

1. Introduction

In recent years, single-molecule detection has been developed for biomedical analysis and diagnosis due to its excellent characteristics of being fast and low-cost and requiring no labeling or sample amplification.[1–7] Particularly, with the quick development of nano-techniques, solid-state nanopores constructed by nanomaterials offer a high-performance platform that significantly reduces the cost and time of single-molecule detection and even sequencing. The principle of nanopore detection/sequencing is that a single nucleotide or single-stranded DNA (ssDNA) is driven through the nanopore by an external stimulus while the corresponding ionic currents are monitored, thus identifying each nucleotide.[8–15] Numerous two-dimensional (2D) nanomaterials, such as graphene,[16–18] hexagonal boron nitride,[19–21] and molybdenum disulfide,[9,10,22] have demonstrated great success in single-molecule detection and sequencing. However, the direct sequencing of ssDNA still suffers from the drawback of significant noise when measuring the ionic current, resulting in high inaccuracy.

To overcome this drawback, a new technology, named exonuclease sequencing has been proposed, which cleaves ssDNA into individual nucleotides followed by single-molecule electrophoretic detection.[23,24] By measuring the TOF of the released nucleotide, the DNA sequence can be identified. Preliminary

[a] School of Physics, Shandong University, Jinan, Shandong 250100, China. E-mail: lxh12345@sdu.edu.cn, xdliu@sdu.edu.cn, lwf@sdu.edu.cn
[b] Key Laboratory for Liquid-Solid Structural Evolution and Processing of Materials, Ministry of Education, Shandong University, Jinan, Shandong 250061, China

experiments and relevant theoretical simulation studies have been conducted. For instance, O'Neil *et al.* investigated the electrokinetic transport properties of dNMPs in thermoplastic nanochannels under different pH and ion concentrations of the electrolyte. A high identification efficiency of greater than 99% was achieved.[25] Later, the same research group used this nanochannel platform for electrokinetic analysis of ribonucleotide monophosphates (rNMPs) and achieved an identification efficiency of higher than 99%.[26] From the theoretical perspective, Moldovanh *et al.* simulated the migration of nucleotides in nanochannels driven by electric fields or water flow and further explored nanochannels modified by chemical surface groups to improve the identification accuracy.[27–29]

The significance of molecular movements in nanofluid is a unique phenomenon associated with this length scale that is distinct from the microscale. When the dimensions are reduced to the nanoscale, the confinement of liquid can cause significant differences in the molecule's apparent mobility that cannot be achieved at the micro- and macroscale. These include enhanced solute/wall interactions due to the small channel diameter, intermittent motion caused by the surface roughness of the channel wall, *etc.* Specifically, controlling the channel surface chemically or physically can lead to clear variations in solute/wall interactions (typically, by enhancement of the binding) such as van der Waals attraction, π–π stacking and hydrophobic interactions of the dNMP and the channel walls, resulting in a broadening of the TOF distribution. Considering this, the development of nanomaterials with strong roughness could be an efficient method for the development and fabrication of high-performance electrophoretic nanochannels.

Recently, a new 2D nanomaterial, α-phase phosphorene carbide (α-PC), has been fabricated and has a unique puckered honeycomb structure.[30–32] Benefitting from its outstanding physical and chemical properties, α-PC has found broad applications in electronic sensors,[33] water filtration,[34] and catalysis.[35] In addition, our previous work demonstrated that the wrinkled surface of α-PC can effectively modulate the migration of proteins. Specifically, a protein can only freely migrate along the zigzag direction (the grooves of α-PC), while migration along the armchair direction is highly prohibited by a large energy barrier.[36] Considering this outstanding structural property, the application of α-PC in electrophoretic detection is expected to effectively regulate the electrokinetic behavior of nucleotides.

In the present work, we studied the transport properties of dNMPs through α-PC nanochannels under an electric field using molecular dynamics simulations. Our results demonstrate that the channel can separate different nucleotides at an appropriate range of electric field strengths. The pattern of the electrophoretic migration velocity of nucleotides along the electric field direction is dTMP > dCMP > dAMP > dGMP, which is in agreement with experimental data.[37] Through the analyses, we found optimized electric field strengths of 0.7–0.8 V nm^{-1} which show considerably high identification accuracy among the four nucleotides. In addition, we found significant differences in the velocities corresponding to the two adsorption conformations of dGMP leading to the largest spreading of the signal in time, which explains the same experimental phenomenon. Our study validates the feasibility of our designed nanodevice and provides a visual interpretation of the experimental results to guide future nano-sensor design and sequencing platform construction.

2. Computational methods

By applying a constant electric field along the x direction, dNMPs were pulled along the armchair direction of the nanochannel. Since the lattice vector of α-PC is 0.851 nm along the armchair direction, which is comparable to the size of a mononucleotide, the nanochannel is believed to be efficient to regulate the migration of nucleotides when they cross the wrinkles. The nanochannel was constructed by stacking 2D α-PC monolayers. Each α-PC layer has dimensions of 5.106 nm × 4.963 nm and is composed of 408 phosphorus and 408 carbon atoms. Due to the winkle structure, α-PC has two representative directions, zigzag and armchair, as labeled in Fig. 1a. The simulation model is depicted in Fig. 1b, where one piece of α-PC nanosheet is placed in the x–y plane and the z-direction of the model box is set to be 2.5–4 nm. With periodic boundary conditions, this setup mimics a nanochannel within two α-PC nanosheets with a height of 2.5 to 4 nm, as demonstrated in Fig. 1b. The dNMP was initially placed in the middle of the α-PC nanochannel. Then, the complex was solvated in a water box. K^+ and Cl^- ions were added to neutralize the net charge of the dNMP and mimic a physiological saline concentration of 0.15 M.

All MD simulations were performed using the GROMACS software package[38] and the molecular structures were visualized by VMD software.[39] The AMBER99sb force field[40] was applied for the dNMPs and their atomic charges were adopted from a previous report by M. Chehelamirani *et al.*[41] For the α-PC nanosheet, the force field parameters were adopted from our previous works.[34,36,42] The TIP3P water model[43] was applied for water and the parameters of K^+ and Cl^- ions were developed by Thomas E. Cheatham *et al.*[44] During the simulation, Newton's equations of motion were integrated using the leap-frog algorithm. The covalent bonds involving hydrogen atoms are constrained by the LINCS algorithm so the time step was set to 2 fs.[45] The van der Waals and short-range Coulomb interactions were handled with a cutoff distance of 1.0 nm, while long-range electrostatic interactions are summed in reciprocal space by the PME method.[46] The simulated system was first optimized for energy minimization using the steepest descent method and then equilibrated for 5 ns under the NVT ensemble (300 K using the V-rescale algorithm[47] for temperature coupling) and the NPT ensemble (300 K and 1 bar using the Parrinello–Rahman algorithm[48] for semi-isotropic pressure coupling along the z direction) to obtain a stable initial configuration. During the equilibration, the heavy atoms of the dNMPs were restrained using harmonic potential. We considered nanochannel widths of 2.5, 3.0, 3.5, and 4 nm for each dNMP with electric field strengths of 0.2, 0.4, 0.6, 0.8, and 1 V nm^{-1} for each width. Ten trajectories of 500 ns were conducted for each case for data collection. For the case of the

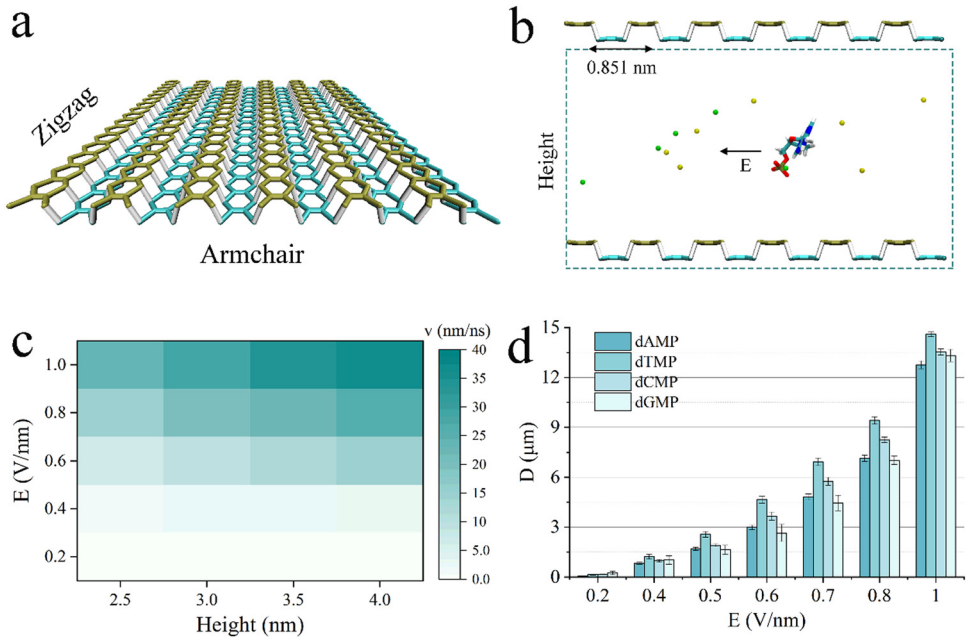

Fig. 1 (a) The crystal structure of α-PC with zigzag and armchair directions labeled. (b) Illustration of the simulation box. The dashed lines indicate periodic boundary conditions. K^+ and Cl^- ions are shown as yellow and green spheres and water is not shown. (c) The velocity of dTMP with respect to nanochannel height from 2.5 to 4.0 nm and electric field strength from 0.2 to 1.0 V nm^{-1}. (d) The total displacement of the four dNMPs after 500 ns simulation along the nanochannel under electric field strengths from 0.2 to 1.0 V nm^{-1}. Each histogram indicates the average value of ten trajectories.

electric field of 0.7 V nm^{-1}, 50 trajectories were collected for more detailed analyses.

3. Results and discussions

3.1. Transport speed of dNMPs in α-PC nanochannel

Ideally, the transport of dNMPs in the α-PC nanochannel is determined by two factors: (1) the height of the nanochannel and (2) the strength of the biasing electric field. Without loss of generality, we first assessed the electrophoretic velocity of dTMP under various conditions. Fig. 1c shows the velocity of dTMP in nanochannels with a height of 2.5 to 4.0 nm and an electric field strength of 0.2 to 1.0 V nm^{-1}. Generally, in the same nanochannel, dTMP transports faster in a stronger electric field. This is expected because dTMP bears a net charge. Moreover, the velocity of dTMP increases when the height of the nanochannel becomes larger. To fully exploit the modulation effect of the nanochannel on the dNMPs, we selected a 3.0 nm height nanochannel and simulated the electrokinetic transport of the four types of dNMPs. Fig. 1d shows the total displacement, D, of the four dNMPs after simulations of 500 ns driven by electric fields from 0.2 to 1.0 V nm^{-1}. This verifies the above observation that the nucleotide moves faster in stronger electric fields. More importantly, it is worth noting that the migration of the four dNMPs shows a clear order under the electric field strengths of 0.5–0.8 V nm^{-1} which is uniformly dTMP > dCMP > dAMP > dGMP. This makes it possible to realize high-precision identification of single nucleotides through monitoring the migration distance or TOF.

To evaluate the accuracy of the α-PC nanochannel for electrophoretic detection, we quantified the differences in the displacements of the four nucleotides by analysis of variance (ANOVA) and the results are summarized in Fig. 2. ANOVA is a statistical method used to determine if there is a significant difference between two or more groups of data. Typically, it is widely accepted that there is a statistically significant difference between the means of the different groups if the *P*-value is less than 0.05. Otherwise, there are not enough statistically significant differences between them. The smaller the *P*-value, the greater the significance of the observed differences. As shown in Fig. 2a and b, at small electric fields from 0.2 to 0.4 V nm^{-1}, the mean D from ten trajectories has large errors and, more importantly, the ordering of their displacement is inconsistent, making it difficult to identify the four dNMPs (two *P*-value > 0.05). When driven by moderate strength electric fields of 0.5–0.8 V nm^{-1} (Fig. 2c–f), the movements of the four dNMPs can be well distinguished from each other, except for dAMP and dGMP, which have similar *D* values. However, when increasing to fifty simulation trajectories for the case of 0.7 V nm^{-1}, the four nucleotides show marked distinctions between each other and thus are more distinguishable (Fig. 2h). Further increment of the electric field strength to 1.0 V nm^{-1} changed the order of the four nucleotides, making the dCMP and dGMP barely distinguishable (Fig. 2g).

Comparing all the electrokinetic data in Fig. 2, we noticed that the displacement of dGMP always has the largest errors. This is believed to be the major reason for the relatively lower identification of dGMP than other dNMPs. Considering this, we explicitly calculated the velocities of the four dNMPs (averaged from 50 trajectories) using the simulations at 0.7 V nm^{-1} as a

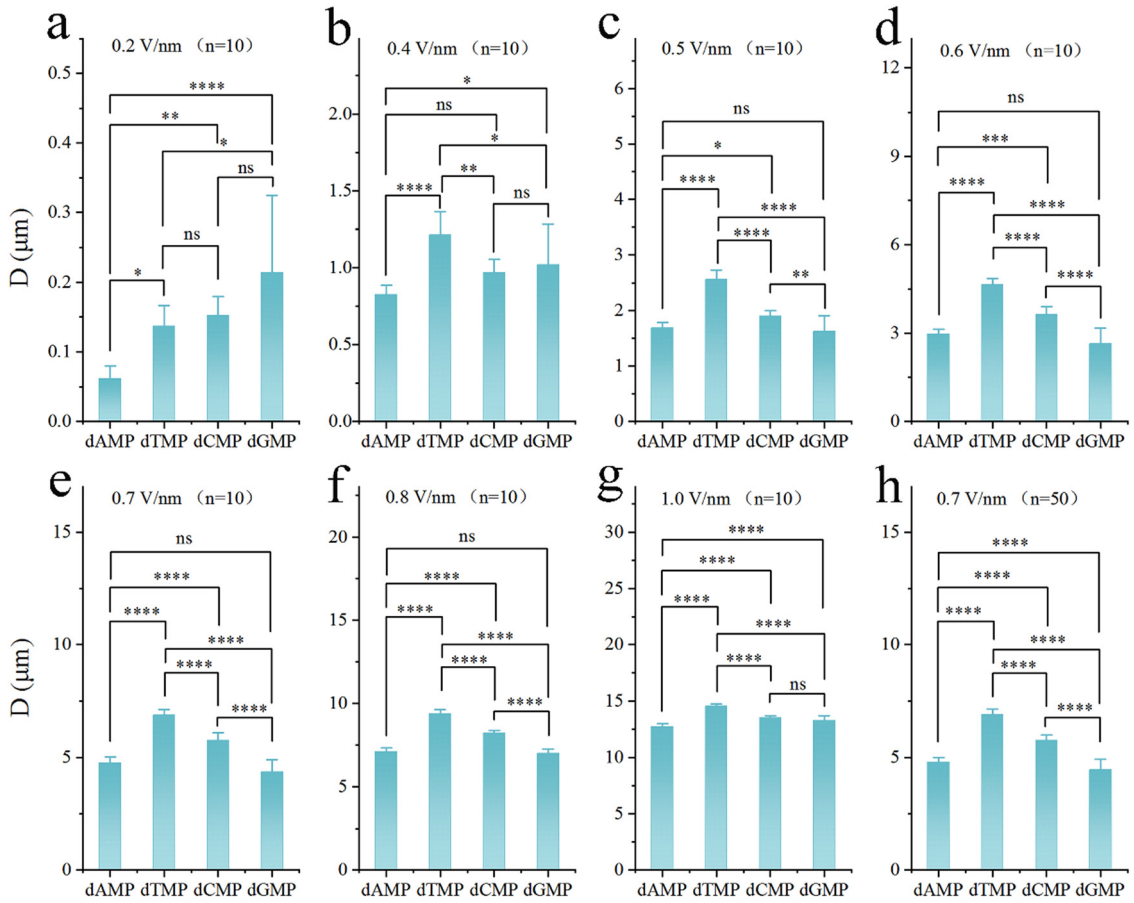

Fig. 2 Analysis of variance (ANOVA) of nucleotide displacement in the 3.0 nm height nanochannel under electric fields: (a–g) data from ten trajectories and (h) an enhanced sampling at 0.7 V nm^{-1} with fifty trajectories. (ns: $P > 0.05$, *: $P \leq 0.05$, **: $P \leq 0.01$, ***: $P \leq 0.001$ and ****: $P \leq 0.0001$).

representative case. In Fig. 3, we present the distribution of the dNMPs' velocities. The velocity distribution curves of dTMP, dCMP, and dAMP are localized and follow the Gaussian distribution. In contrast, the velocity distribution curve of dGMP spreads from around 7 to 10 nm ns^{-1} and has several peaks. For instance, there are two obvious peaks at 8.80 and 10.02 nm ns^{-1}. Excitingly, our findings are in good agreement with the experimental report by Choi *et al.*, who also found a broad distribution when monitoring the TOF of dGMP by 5 μm nanochannel electrophoresis, but did not identify the reason.[37]

3.2. Binding patterns of dNMPs on α-PC Surface

The broad distribution of the velocity of dGMP is the major obstacle to accurate identification of the four nucleotides under the same electric field. Considering that the distribution of the dGMP velocity is composed of two Gaussian curves, we speculate that dGMP might have more complicating binding patterns on the α-PC surface than the other three dNMPs, resulting in distinct velocities in the channel. To validate our hypothesis, we analyzed the binding states of the dNMPs on the α-PC surface. Because of the aromatic structure of the nucleobase, its adsorption on the α-PC surface is mainly through π–π stacking interactions. The two sides of the nucleobase can both bind to the α-PC surface and these orientations are termed 5′ contact and 3′ contact. Representative binding structures of the

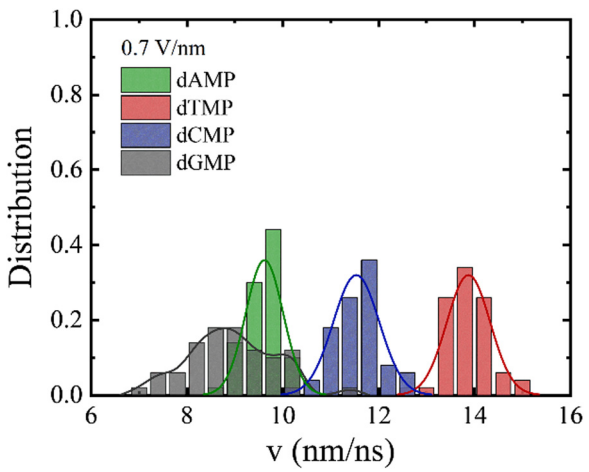

Fig. 3 Distribution of dNMP velocities in the nanochannel at an electric field strength of 0.7 V nm^{-1}. (A total of 50 simulation trajectories of 500 ns were used for each dNMP.)

two states are depicted in Fig. 4a and b, respectively. We further defined a non-contact state to represent the isolated nucleotide in solution inside the channel.

To roughly describe the binding strengths of the two orientations, we calculated the minimum distance of the P atom on the

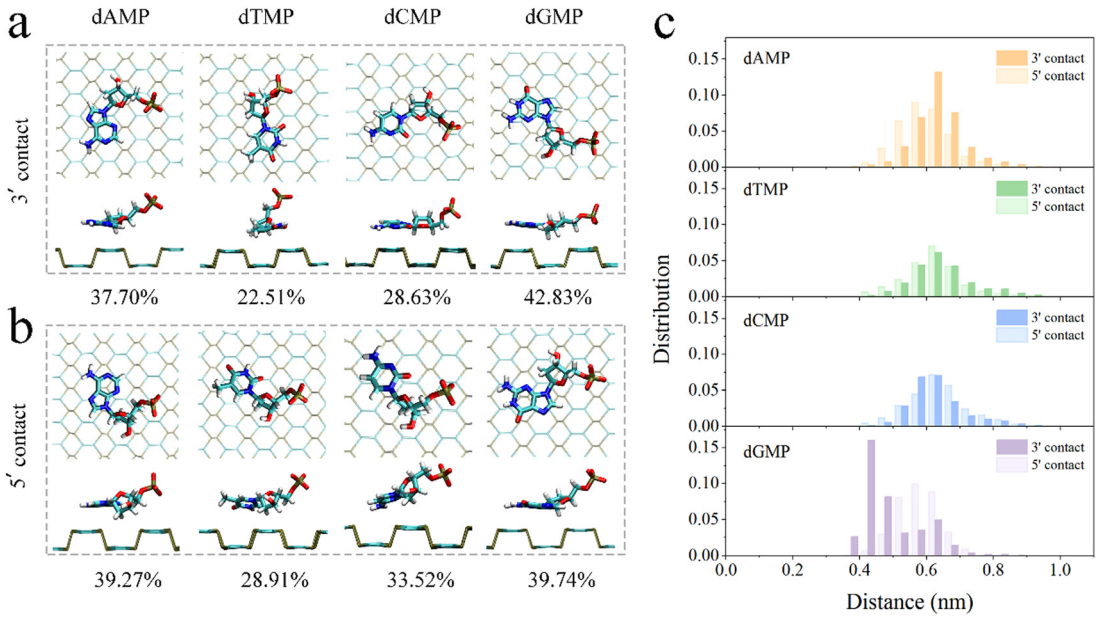

Fig. 4 Top and side views of the (a) 3′ contact state and (b) 5′ contact state of the nucleotides binding to α-PC. The value at the bottom of each figure depicts the percentage of the respective state in the whole trajectory. (c) Distributions of the minimum distances of P atoms of nucleotides to α-PC in two adsorption states (simulations conducted at 0.7 V nm^{-1}).

backbone phosphate to α-PC and the distributions are summarized in Fig. 4c. For dAMP, dTMP, and dCMP, the distances are mostly the same, around 0.6 nm, independent of the binding orientation. The only exception is dGMP, where the distance was 0.55 nm in the 5′ contact state and only 0.45 nm in the 3′ contact state. Therefore, dGMP formed a closer binding to α-PC than the other three dNMPs.

3.3. Electrokinetic velocities of dNMPs with different binding orientations

The instantaneous velocity data were classified according to the adsorption states (5′ contact, 3′ contact, and non-contact) of the dNMPs and their distribution histograms are plotted in Fig. 5. Three points can be noted.

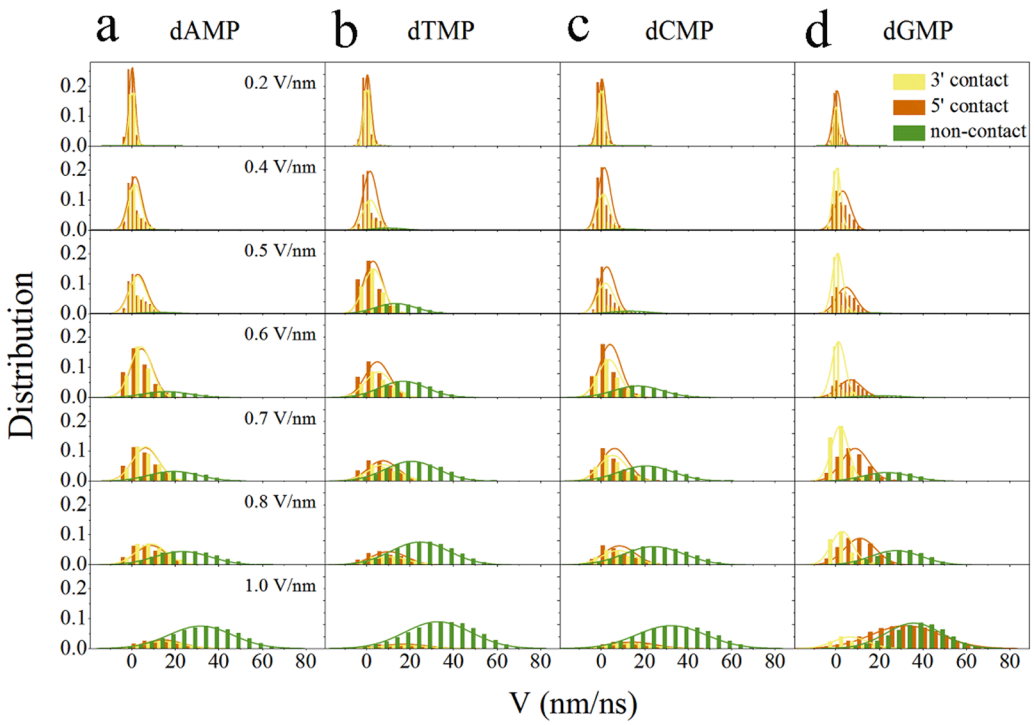

Fig. 5 (a–d) Distribution of nucleotide velocities classified by the adsorption statuses of 3′ contact, 5′ contact and non-contact state.

1. For the four dNMPs in the non-contact state, the velocities are all larger than those in the contact states. This is expected because this case represents the free movement of nucleotides in solvent instead of drifting on the wrinkled α-PC surface.

2. For dAMP, dTMP, and dCMP, the velocity distributions are almost the same for the two binding states from 0.2 to 1.0 V nm^{-1} in either 5′ contact or 3′ contact. This results in well-determined overall velocities for all simulations.

3. dGMP moves faster in the 5′ contact state than in the 3′ contact state. This becomes more significant in large electric fields. The velocity of the 5′ contact state also has a broad distribution. This results in a large uncertainty in the total speed.

Summarizing the above analyses, the factors affecting the total velocity of the nucleotides involve (1) the electrophoretic velocities of the three adsorption states and (2) the corresponding probabilities. To quantitatively demonstrate the velocities of the dNMPs at various electric field strengths, we plotted the average velocities of the three adsorption states with respect to electric field strength in Fig. 6a. At the same adsorption states (3′ or 5′ contact) and electric fields, there are very small differences in the velocities among the four nucleotides. The only exception is dGMP, which has a slightly smaller velocity in the 3′ contact state. Moreover, the velocities of the non-contact state were almost twice those in the contact states. Thus, it is safe to conclude that the overall probabilities of the three states (3′ contact, 5′ contact and non-contact) for the dNMPs inside the nanochannel are the dominant factor for the electrophoretic determination of nucleotides, especially for the non-contact state. In Fig. 6b, we show the probability of nucleotides in the non-contact state with respect to the strength of the electric field. In the weak electric field of 0.2 V nm^{-1}, the dNMPs prefer to bind to the α-PC surface, thus the percentage of the non-contact state is 0. With increasing electric field strength, the non-contact state becomes dominant. This reflects the fact that the dNMPs dissolve from the α-PC surface at strong electric fields because of the greater transport speed effectively inhibiting dNMP binding. It is interesting to find a clear order for the four nucleotides in the non-contact state, which is dTMP > dCMP > dAMP > dGMP for electric fields from 0.4 to 1.0 V nm^{-1}. The overall electrophoretic velocities at different electric field strengths are shown in Fig. 6c. The probability of the nucleotide adsorption state has a significant influence on the final velocity. This further highlights the significance of the nanosurface, which regulates the nucleotide binding states through specific interactions. The probability of desorption of the nucleotides to the non-contact state and the final electrophoretic velocity were both ranked in the order dTMP > dCMP > dAMP > dGMP. We highlight an appropriate range for the electric field, 0.7–0.8 V nm^{-1}, where the total velocities of the four dNMPs can be distinguished.

We also note that the above results are based on α-PC with an ideal structure. However, nanostructures are usually rich in surface defects[49,50] and surface charges,[51,52] which can significantly influence the adsorption and diffusion of biomolecules

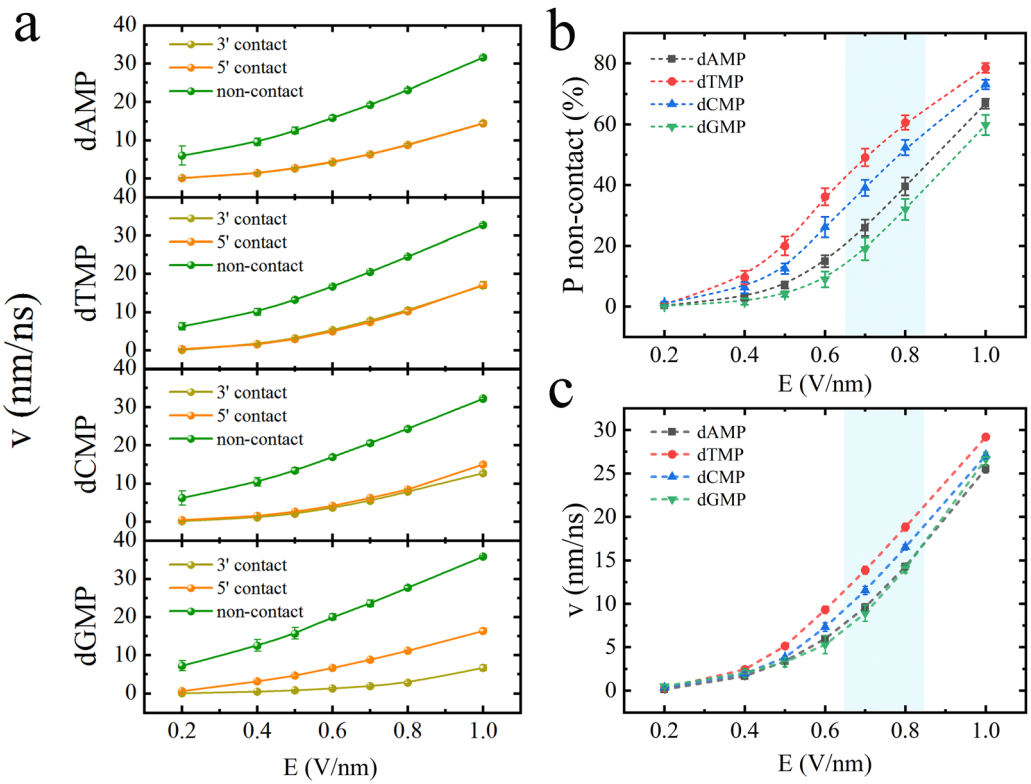

Fig. 6 (a) The velocity of dNMP in different adsorption states with respect to the electric field strength. (b) The probability of the non-contact state of dNMP with respect to electric field strength. (c) The overall velocity of dNMP with respect to electric field strength.

on the surface. Furthermore, surface roughness[29] and chemical modification[28] can also affect the interactions of biomolecules with nanostructures. The effects of these factors on the sensing accuracy of the nanodevice certainly deserve further study.

The winkled surface is an intrinsic property of α-PC that does not require pre-treatments or structural engineering. This is an advantage for practical applications. In addition to detection of dNMPs, the α-PC nanochannel can also be utilized in the separation/detection of DNA and other biomolecules that can be driven by an external stimulus to pass through the nanochannel with a recorded time of flight (TOF). As DNA and biomolecules usually bear a net charge, the stimulus is usually an electric field. Thus, the TOF is dependent on the charge with respect to the molecular mass. Finally, we discuss the possibility of constructing nanochannel devices using α-PC. Thanks to the rapid development of nanotechnology, several convenient methods have been developed for constructing nanochannels using 2D nanomaterials, including vacuum filtration,[53] pressure-assisted filtration,[54] and the wet spinning assembly technique.[55] Additionally, the interlayer spacing of the nanostructures can be precisely controlled.[56–59] This makes it possible to construct a nanochannel by stacking α-PC layers with the desired separation.

4. Conclusion

Using MD simulations, we studied the theoretical electrokinetic transport of nucleotides in α-PC nanochannels. Our results show that dNMPs can be efficiently separated through α-PC nanochannels with an electrophoretic migration velocity order of dTMP > dCMP > dAMP > dGMP in a large range of electric field strengths from 0.5 to 0.8 V nm^{-1}. In an optimized electric field of 0.7 to 0.8 V nm^{-1}, accurate identification of the four nucleotides can be expected. Attributed to the specific binding patterns and interactions of the nucleotide with the wrinkled surface of α-PC, the transport velocity of dNMPs can be well-regulated to ensure accurate detection. We also propose that the dGMP is the weakest link among the four dNMPs for experiments because its velocity always shows a broader distribution. This is because dGMP has significantly different velocities when bound to α-PC in different orientations. In contrast, dAMP, dTMP, and dCMP have almost the same velocity regardless of the binding pattern. The advantage of α-PC for practical applications is that the winkle structure is an intrinsic property that does not require pre-treatments or structural engineering. The wrinkled structure can form different interaction modes with nucleotides that greatly regulate the transport velocities. This should also work for other types of biomolecules. Thus, α-PC can also be used in the design of nanodevices for biochemical and chemical molecular analysis. The present findings validate the feasibility of winkled nanostructures in the design of nanodevices for electrophoretic detection and can be generalized for the design and fabrication of nano-sensors in biological and medical analyses with high detection accuracy.

Conflicts of interest

There are no conflicts to declare.

Acknowledgements

This work is supported by the Natural Science Foundation of Shandong Province (ZR2020JQ04), the National Natural Science Foundation of China (No. 12175126), and the Local Science and Technology Development Fund Guided by the Central Government of Shandong Province (YDZX2022089).

References

1 B. Luan and R. Zhou, *ACS Nano*, 2018, **12**, 3886–3891.
2 Y. P. Shan, P. B. Tiwari, P. Krishnakumar, I. Vlassiouk, W. Z. Li, X. W. Wang, Y. Darici, S. M. Lindsay, H. D. Wang, S. Smirnov and J. He, *Nanotechnology*, 2013, **24**, 495102.
3 S. Liu, B. Lu, Q. Zhao, J. Li, T. Gao, Y. Chen, Y. Zhang, Z. Liu, Z. Fan, F. Yang, L. You and D. Yu, *Adv. Mater.*, 2013, **25**, 4549–4554.
4 H. Ouldali, K. Sarthak, T. Ensslen, F. Piguet, P. Manivet, J. Pelta, J. C. Behrends, A. Aksimentiev and A. Oukhaled, *Nat. Biotechnol.*, 2020, **38**, 176–181.
5 Y. Lu, X. Y. Wu, Y. L. Ying and Y. T. Long, *Chem. Commun.*, 2019, **55**, 9311–9314.
6 C. A. Amarasekara, U. S. Athapattu, C. Rathnayaka, J. Choi, S. Park and S. A. Soper, *Electrophoresis*, 2020, **41**, 1627–1640.
7 G. Huang, K. Willems, M. Soskine, C. Wloka and G. Maglia, *Nat. Commun.*, 2017, **8**, 935.
8 H. Qiu, A. Sarathy, J. P. Leburton and K. Schulten, *Nano Lett.*, 2015, **15**, 8322–8330.
9 M. Xiong, M. Graf, N. Athreya, A. Radenovic and J.-P. Leburton, *ACS Nano*, 2020, **14**, 16131–16139.
10 J. Feng, K. Liu, R. D. Bulushev, S. Khlybov, D. Dumcenco, A. Kis and A. Radenovic, *Nat. Nanotechnol.*, 2015, **10**, 1070–1076.
11 R. K. Sharma, I. Agrawal, L. Dai, P. Doyle and S. Garaj, *Nano Lett.*, 2021, **21**, 3772–3779.
12 J. Wilson, L. Sloman, Z. He and A. Aksimentiev, *Adv. Funct. Mater.*, 2016, **26**, 4830–4838.
13 S. Su, X. Wang and J. Xue, *Mater. Horiz.*, 2021, **8**, 1390–1408.
14 M. Zhang, S. Chen, J. Hu, Q. Ding, L. Li, S. Lü and M. Long, *Nanoscale*, 2021, **13**, 6053–6065.
15 Y. Liu, Y. Deng, Y. Yang, Y. Qu, C. Zhang, Y.-Q. Li, M. Zhao and W. Li, *Nanoscale Adv.*, 2021, **3**, 5941–5947.
16 S. Banerjee, J. Wilson, J. Shim, M. Shankla, E. A. Corbin, A. Aksimentiev and R. Bashir, *Adv. Funct. Mater.*, 2015, **25**, 936–946.
17 S. M. Avdoshenko, D. Nozaki, C. Gomes da Rocha, J. W. Gonzalez, M. H. Lee, R. Gutierrez and G. Cuniberti, *Nano Lett.*, 2013, **13**, 1969–1976.
18 G. F. Schneider, S. W. Kowalczyk, V. E. Calado, G. Pandraud, H. W. Zandbergen, L. M. K. Vandersypen and C. Dekker, *Nano Lett.*, 2010, **10**, 3163–3167.
19 A. Smolyanitsky and B. Luan, *Phys. Rev. Lett.*, 2021, **127**, 138103.

20 B. Luan and R. Zhou, *Nano Lett.*, 2019, **19**, 977–982.
21 Z. Zhou, Y. Hu, H. Wang, Z. Xu, W. Wang, X. Bai, X. Shan and X. Lu, *Sci. Rep.*, 2013, **3**, 3287.
22 A. B. Farimani, K. Min and N. R. Aluru, *ACS Nano*, 2014, **8**, 7914–7922.
23 K. T. Brady and J. E. Reiner, *J. Chem. Phys.*, 2015, **143**, 074904.
24 N. J. Oliver-Calixte, F. I. Uba, K. N. Battle, K. M. Weerakoon-Ratnayake and S. A. Soper, *Anal. Chem.*, 2014, **86**, 4447–4454.
25 C. O'Neil, C. A. Amarasekara, K. M. Weerakoon-Ratnayake, B. Gross, Z. Jia, V. Singh, S. Park and S. A. Soper, *Anal. Chim. Acta*, 2018, **1027**, 67–75.
26 C. A. Amarasekara, C. Rathnayaka, U. S. Athapattu, L. Zhang, J. Choi, S. Park, A. C. Nagel and S. A. Soper, *J. Chromatogr. A*, 2021, **1638**, 461892.
27 B. R. Novak, D. Moldovan, D. E. Nikitopoulos and S. A. Soper, *J. Phys. Chem. B*, 2013, **117**, 3271–3279.
28 X. Tong, B. R. Novak, S. Kavousi and D. Moldovan, *J. Phys. Chem. B*, 2021, **125**, 1259–1270.
29 K. Xia, B. R. Novak, K. M. Weerakoon-Ratnayake, S. A. Soper, D. E. Nikitopoulos and D. Moldovan, *J. Phys. Chem. B*, 2015, **119**, 11443–11458.
30 W. C. Tan, Y. Cai, R. J. Ng, L. Huang, X. Feng, G. Zhang, Y.-W. Zhang, C. A. Nijhuis, X. Liu and K.-W. Ang, *Adv. Mater.*, 2017, **29**, 1700503.
31 W. C. Tan, L. Huang, R. J. Ng, L. Wang, D. M. N. Hasan, T. J. Duffin, K. S. Kumar, C. A. Nijhuis, C. Lee and K.-W. Ang, *Adv. Mater.*, 2018, **30**, 1705039.
32 X. Huang, Y. Cai, X. Feng, W. C. Tan, D. M. N. Hasan, L. Chen, N. Chen, L. Wang, L. Huang, T. J. Duffin, C. A. Nijhuis, Y.-W. Zhang, C. Lee and K.-W. Ang, *ACS Photonics*, 2018, **5**, 3116–3123.
33 S. Qi, F. Li, J. Wang, Y. Qu, Y. Yang, W. Li and M. Zhao, *Carbon*, 2019, **141**, 444–450.
34 Y. Li, Y. Liu, Y. Yang, Y.-Q. Li, M. Zhao, W. Li and Y. Qu, *Desalination*, 2022, **522**, 115422.
35 D. Chen, Z. Chen, X. Zhang, Z. Lu, S. Xiao, B. Xiao and C. V. Singh, *J. Energy Chem.*, 2021, **52**, 155–162.
36 Y. Liu, X. Song, Y. Yang, Y. Q. Li, M. Zhao, Y. Mu and W. Li, *Nanoscale*, 2020, **12**, 5209–5216.
37 J. Choi, Z. Jia, R. Riahipour, C. J. McKinney, C. A. Amarasekara, K. M. Weerakoon-Ratnayake, S. A. Soper and S. Park, *Small*, 2021, **17**, 2102567.
38 M. J. Abraham, T. Murtola, R. Schulz, S. Páll, J. C. Smith, B. Hess and E. Lindahl, *SoftwareX*, 2015, **1–2**, 19–25.
39 W. Humphrey, A. Dalke and K. Schulten, *J. Mol. Graphics Modell.*, 1996, **14**, 33–38.
40 K. Lindorff-Larsen, S. Piana, K. Palmo, P. Maragakis, J. L. Klepeis, R. O. Dror and D. E. Shaw, *Proteins*, 2010, **78**, 1950–1958.
41 M. Chehelamirani and T. Tang, *Mol. Simul.*, 2017, **43**, 610–624.
42 Y. Liu, Y. Yang, Y. Qu, Y.-Q. Li, M. Zhao and W. Li, *Phys. Chem. Chem. Phys.*, 2020, **22**, 23268–23275.
43 W. L. Jorgensen, J. Chandrasekhar, J. D. Madura, R. W. Impey and M. L. Klein, *J. Chem. Phys.*, 1983, **79**, 926–935.
44 I. S. Joung and T. E. Cheatham, *J. Phys. Chem. B*, 2008, **112**, 9020–9041.
45 B. Hess, H. Bekker, H. J. C. Berendsen and J. Fraaije, *J. Comput. Chem.*, 1997, **18**, 1463–1472.
46 U. Essmann, L. Perera, M. L. Berkowitz, T. Darden, H. Lee and L. G. Pedersen, *J. Chem. Phys.*, 1995, **103**, 8577–8593.
47 G. Bussi, D. Donadio and M. Parrinello, *J. Chem. Phys.*, 2007, **126**, 014101.
48 S. Nosé and M. L. Klein, *Mol. Phys.*, 2006, **50**, 1055–1076.
49 Z. Gu, W. Song, S. H. Chen, B. Li, W. Li and R. Zhou, *Nanoscale*, 2019, **11**, 19362–19369.
50 B. Li, D. R. Bell, Z. Gu, W. Li and R. Zhou, *Carbon*, 2019, **146**, 257–264.
51 Y. Deng, F. Wang, Y. Liu, Y. Yang, Y. Qu, M. Zhao, Y. Mu and W. Li, *Nanoscale*, 2020, **12**, 5217–5226.
52 X. Jia, Y. Yang, Y. Liu, W. Niu, Y.-Q. Li, M. Zhao, Y. Mu and W. Li, *Nanoscale Adv.*, 2020, **2**, 4539–4546.
53 K. Raidongia and J. Huang, *J. Am. Chem. Soc.*, 2012, **134**, 16528–16531.
54 C.-H. Tsou, Q.-F. An, S.-C. Lo, M. De Guzman, W.-S. Hung, C.-C. Hu, K.-R. Lee and J.-Y. Lai, *J. Membr. Sci.*, 2015, **477**, 93–100.
55 Z. Liu, Z. Li, Z. Xu, Z. Xia, X. Hu, L. Kou, L. Peng, Y. Wei and C. Gao, *Chem. Mater.*, 2014, **26**, 6786–6795.
56 W. Li, W. Wu and Z. Li, *ACS Nano*, 2018, **12**, 9309–9317.
57 E. M. Mannebach, C. Nyby, F. Ernst, Y. Zhou, J. Tolsma, Y. Li, M. J. Sher, I. C. Tung, H. Zhou, Q. Zhang, K. L. Seyler, G. Clark, Y. Lin, D. Zhu, J. M. Glownia, M. E. Kozina, S. Song, S. Nelson, A. Mehta, Y. Yu, A. Pant, B. Aslan, A. Raja, Y. Guo, A. DiChiara, W. Mao, L. Cao, S. Tongay, J. Sun, D. J. Singh, T. F. Heinz, X. Xu, A. H. MacDonald, E. Reed, H. Wen and A. M. Lindenberg, *Nano Lett.*, 2017, **17**, 7761–7766.
58 S. Wang, Y. Wu, N. Zhang, G. He, Q. Xin, X. Wu, H. Wu, X. Cao, M. D. Guiver and Z. Jiang, *Energy Environ. Sci.*, 2016, **9**, 3107–3112.
59 S. Wang, L. Yang, G. He, B. Shi, Y. Li, H. Wu, R. Zhang, S. Nunes and Z. Jiang, *Chem. Soc. Rev.*, 2020, **49**, 1071–1089.